Charge-Transfer and Spin Dynamics in DNA Hairpin Conjugates with Perylenediimide as a Base-Pair Surrogate

ARTICLE *in* JOURNAL OF THE AMERICAN CHEMICAL SOCIETY · OCTOBER 2008

Impact Factor: 12.11 · DOI: 10.1021/ja803765r · Source: PubMed

6 AUTHORS, INCLUDING:

Raanan Carmielli
Weizmann Institute of Science
44 PUBLICATIONS **877** CITATIONS

SEE PROFILE

Frederick D Lewis
Northwestern University
319 PUBLICATIONS **9,191** CITATIONS

SEE PROFILE

J|A|C|S
ARTICLES

Published on Web 09/24/2008

Charge-Transfer and Spin Dynamics in DNA Hairpin Conjugates with Perylenediimide as a Base-Pair Surrogate

Tarek A. Zeidan, Raanan Carmieli, Richard F. Kelley, Thea M. Wilson, Frederick D. Lewis,* and Michael R. Wasielewski*

Department of Chemistry and Argonne−Northwestern Solar Energy Research (ANSER) Center, Northwestern University, Evanston, Illinois 60208-3113

Received May 20, 2008; E-mail: fdl@northwestern.edu; m-wasielewski@northwestern.edu

Abstract: A perylenediimide chromophore (P) was incorporated into DNA hairpins as a base-pair surrogate to prevent the self-aggregation of P that is typical when it is used as the hairpin linker. The photoinduced charge-transfer and spin dynamics of these hairpins were studied using femtosecond transient absorption spectroscopy and time-resolved EPR spectroscopy (TREPR). P is a photooxidant that is sufficiently powerful to quantitatively inject holes into adjacent adenine (A) and guanine (G) nucleobases. The charge-transfer dynamics observed following hole injection from P into the A-tract of the DNA hairpins is consistent with formation of a polaron involving an estimated 3−4 A bases. Trapping of the $(A_{3-4})^{+\bullet}$ polaron by a G base at the opposite end of the A-tract from P is competitive with charge recombination of the polaron and $P^{-\bullet}$ only at short P−G distances. In a hairpin having 3 A−T base pairs between P and G (**4G**), the radical ion pair that results from trapping of the hole by G is spin-correlated and displays TREPR spectra at 295 and 85 K that are consistent with its formation from ^{1*}P by the radical-pair intersystem crossing mechanism. Charge recombination is spin-selective and produces ^{3*}P, which at 85 K exhibits a spin-polarized TREPR spectrum that is diagnostic of its origin from the spin-correlated radical ion pair. Interestingly, in a hairpin having no G bases (**0G**), TREPR spectra at 85 K revealed a spin-correlated radical pair with a dipolar interaction identical to that of **4G**, implying that the A-base in the fourth A−T base pair away from the P chromophore serves as a hole trap. Our data suggest that hole injection and transport in these hairpins is completely dominated by polaron generation and movement to a trap site rather than by superexchange. On the other hand, the barrier for charge injection from $G^{+\bullet}$ back onto the A−T base pairs is strongly activated, so charge recombination from G (or even A trap sites at 85 K) most likely proceeds by a superexchange mechanism.

Introduction

Perylene-3,4:9,10-bis(dicarboximide) (PDI) and its derivatives have attracted significant interest as active materials for light harvesting,[1−5] photovoltaics,[6−13] and studies of basic photoinduced charge- and energy-transfer processes.[14−19] PDI is both photochemically and thermally stable[20] and can be easily modified at its imide nitrogens and its 1, 6, 7, and 12 positions. PDI also demonstrates the ability to self-assemble in solution via hydrophobic/hydrophilic interactions as well as by $\pi-\pi$ stacking.[21−43] Bis(oligonucleotide) conjugates having PDI link-

(1) Prathapan, S.; Yang, S. I.; Seth, J.; Miller, M. A.; Bocian, D. F.; Holten, D.; Lindsey, J. S. *J. Phys. Chem. B* **2001**, *105*, 8237–8248.
(2) Yang, S. I.; Prathapan, S.; Miller, M. A.; Seth, J.; Bocian, D. F.; Lindsey, J. S.; Holten, D. *J. Phys. Chem. B* **2001**, *105*, 8249–8258.
(3) Tomizaki, K.; Loewe, R. S.; Kirmaier, C.; Schwartz, J. K.; Retsek, J. L.; Bocian, D. F.; Holten, D.; Lindsey, J. S. *J. Org. Chem.* **2002**, *67*, 6519–6534.
(4) Muthukumaran, K.; Loewe, R. S.; Kirmaier, C.; Hindin, E.; Schwartz, J. K.; Sazanovich, I. V.; Diers, J. R.; Bocian, D. F.; Holten, D.; Lindsey, J. S. *J. Phys. Chem. B* **2003**, *107*, 3431–3442.
(5) Miller, M. A.; Lammi, R. K.; Prathapan, S.; Holten, D.; Lindsey, J. S. *J. Org. Chem.* **2000**, *65*, 6634–6649.
(6) Chen, S.-G.; Stradins, P.; Gregg, B. A. *J. Phys. Chem. B* **2005**, *109*, 13451–13460.
(7) Chen, S. G.; Branz, H. M.; Eaton, S. S.; Taylor, P. C.; Cormier, R. A.; Gregg, B. A. *J. Phys. Chem. B* **2004**, *108*, 17329–17336.
(8) Gregg, B. A. *J. Phys. Chem. B* **2003**, *107*, 4688–4698.
(9) Neuteboom, E. E.; Meskers, S. C. J.; Van Hal, P. A.; Van Duren, J. K. J.; Meijer, E. W.; Janssen, R. A. J.; Dupin, H.; Pourtois, G.; Cornil, J.; Lazzaroni, R.; Bredas, J.-L.; Beljonne, D. *J. Am. Chem. Soc.* **2003**, *125*, 8625–8638.
(10) Gregg, B. A.; Cormier, R. A. *J. Am. Chem. Soc.* **2001**, *123*, 7959–7960.
(11) Dittmer, J. J.; Marseglia, E. A.; Friend, R. H. *Adv. Mater.* **2000**, *12*, 1270–1274.
(12) Ferrere, S.; Zaban, A.; Gregg, B. A. *J. Phys. Chem. B* **1997**, *101*, 4490–4493.
(13) Tang, C. W. *Appl. Phys. Lett.* **1986**, *48*, 183–185.
(14) Ford, W. E.; Kamat, P. V. *J. Phys. Chem.* **1987**, *91*, 6373–6380.
(15) Ford, W. E.; Hiratsuka, H.; Kamat, P. V. *J. Phys. Chem.* **1989**, *93*, 6692–6696.
(16) Würthner, F.; Thalacker, C.; Sautter, A. *Adv. Mater.* **1999**, *11*, 754–758.
(17) Langhals, H.; Saulich, S. *Chem.—Eur. J.* **2002**, *8*, 5630–5643.
(18) Schenning, A. P. H. J.; van Herrikhuyzen, J.; Jonkheijm, P.; Chen, Z.; Würthner, F.; Meijer, E. W. *J. Am. Chem. Soc.* **2002**, *124*, 10252–10253.
(19) Kirmaier, C.; Hindin, E.; Schwartz, J. K.; Sazanovich, I. V.; Diers, J. R.; Muthukumaran, K.; Taniguchi, M.; Bocian, D. F.; Lindsey, J. S.; Holten, D. *J. Phys. Chem. B* **2003**, *107*, 3443–3454.
(20) Langhals, H.; Ismael, R. *Eur. J. Org. Chem.* **1998**, 1915–1917.
(21) Ahrens, M. J.; Sinks, L. E.; Rybtchinski, B.; Liu, W.; Jones, B. A.; Giaimo, J. M.; Gusev, A. V.; Goshe, A. J.; Tiede, D. M.; Wasielewski, M. R. *J. Am. Chem. Soc.* **2004**, *126*, 8284–8294.
(22) Thalacker, C.; Würthner, F. *Adv. Funct. Mater.* **2002**, *12*, 209–218.

Chart 1. Structures of DNA Hairpins and Reference Molecules

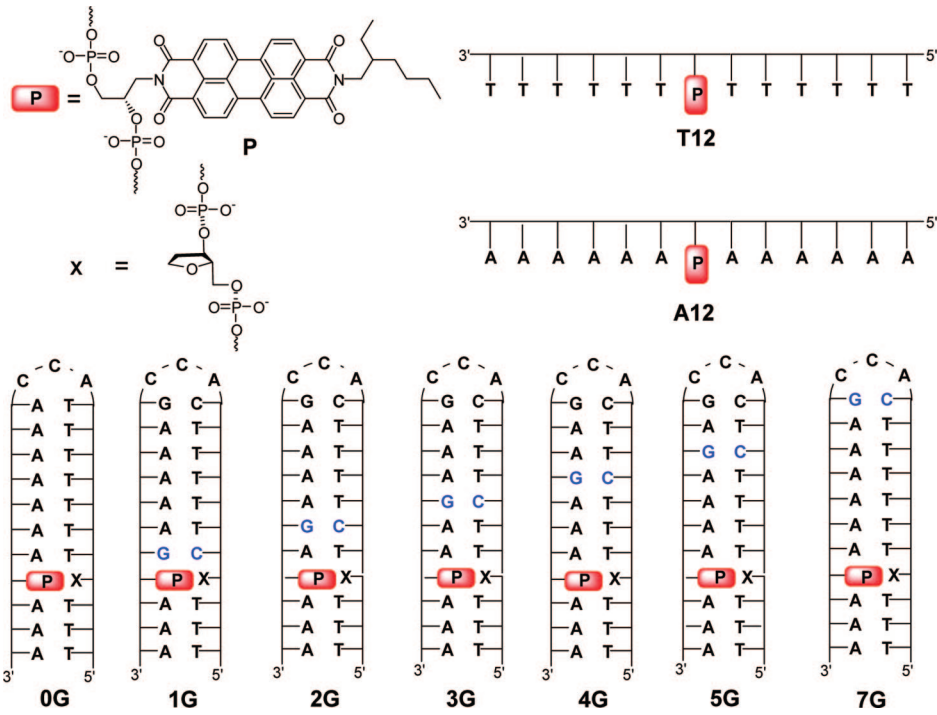

ers have been reported to form a variety of structures, including hairpins, hairpin dimers, duplexes, dumbbells, triplexes, and foldamers.[44−51] Several of these reports have noted that the strong fluorescence characteristic of the unmodified PDI chromophore is largely quenched in its DNA conjugates, presumably as a consequence of photoinduced electron transfer from the nucleobases to singlet PDI. Investigation of the dynamics and mechanism of photoinduced electron transfer in these conjugates is complicated by the propensity of hydrophobic PDI to form aggregates in aqueous solution.[49,50] Wagner and Wagenknecht[52] recently reported the preparation of the PDI derivative P (Chart 1), which can be incorporated into an oligonucleotide and serve as a base-pair surrogate when located opposite an abasic site in a duplex structure. Self-aggregation of P is precluded by these duplex structures, yet the fluorescence of P is effectively quenched. These results suggested to us that P could be employed as a base-pair replacement within the DNA duplex to investigate photoinduced electron transfer without the complications introduced by PDI self-aggregation when PDI itself serves as the hairpin linker.[46]

We report here the results of our investigation of the dynamics and mechanism of photoinduced electron transfer in a series of synthetic DNA hairpins ***n*G** ($n = 0-5, 7$) (Chart 1). These hairpins possess compact 3′-CCA loop regions connecting

(23) van der Boom, T.; Hayes, R. T.; Zhao, Y.; Bushard, P. J.; Weiss, E. A.; Wasielewski, M. R. *J. Am. Chem. Soc.* **2002**, *124*, 9582–9590.
(24) Wang, W.; Li, L. S.; Helms, G.; Zhou, H. H.; Li, A. D. Q. *J. Am. Chem. Soc.* **2003**, *125*, 1120–1121.
(25) Wang, W.; Han, J. J.; Wang, L. Q.; Li, L. S.; Shaw, W. J.; Li, A. D. Q. *Nano Lett.* **2003**, *3*, 455–458.
(26) Würthner, F. *Chem. Commun.* **2004**, 1564–1579.
(27) Yan, P.; Chowdhury, A.; Holman, M. W.; Adams, D. M. *J. Phys. Chem. B* **2005**, *109*, 724–730.
(28) Han, J. J.; Wang, W.; Li, A. D. Q. *J. Am. Chem. Soc.* **2006**, *128*, 672–673.
(29) Neuteboom, E. E.; Meskers, S. C. J.; Meijer, E. W.; Janssen, R. A. J. *Macromol. Chem. Phys.* **2004**, *205*, 217–222.
(30) Datar, A.; Oitker, R.; Zang, L. *Chem. Commun.* **2006**, 1649–1651.
(31) Dehm, V.; Chen, Z.; Baumeister, U.; Prins, P.; Siebbeles, L. D. A.; Würthner, F. *Org. Lett.* **2007**, *9*, 1085–1088.
(32) Zhan, X.; Tan, Z.'a.; Domercq, B.; An, Z.; Zhang, X.; Barlow, S.; Li, Y.; Zhu, D.; Kippelen, B.; Marder, S. R. *J. Am. Chem. Soc.* **2007**, *129*, 7246–7247.
(33) Che, Y.; Datar, A.; Balakrishnan, K.; Zang, L. *J. Am. Chem. Soc.* **2007**, *129*, 7234–7235.
(34) Che, Y.; Datar, A.; Yang, X.; Naddo, T.; Zhao, J.; Zang, L. *J. Am. Chem. Soc.* **2007**, *129*, 6354–6355.
(35) Yagai, S.; Monma, Y.; Kawauchi, N.; Karatsu, T.; Kitamura, A. *Org. Lett.* **2007**, *9*, 1137–1140.
(36) Würthner, F.; Hanke, B.; Lysetska, M.; Lambright, G.; Harms, G. S. *Org. Lett.* **2005**, *7*, 967–970.
(37) Würthner, F.; Sautter, A. *Chem. Commun.* **2000**, 445–446.
(38) Kaiser, T. E.; Wang, H.; Stepanenko, V.; Würthner, F. *Angew. Chem., Int. Ed.* **2007**, *46*, 5541–5544.
(39) Chen, Z.; Baumeister, U.; Tschierske, C.; Würthner, F. *Chem.—Eur. J.* **2007**, *13*, 450–465.
(40) Li, X. Y.; Sinks, L. E.; Rybtchinski, B.; Wasielewski, M. R. *J. Am. Chem. Soc.* **2004**, *126*, 10810–10811.
(41) Zhang, J.; Hoeben, F. J. M.; Pouderoijen, M. J.; Schenning, A. P. H.; Meijer, E. W.; Schryver, F. C.; De Feyter, S. *Chem.—Eur. J.* **2006**, *12*, 9046–9055.
(42) Rybtchinski, B.; Sinks, L. E.; Wasielewski, M. R. *J. Phys. Chem. A* **2004**, *108*, 7497–7505.
(43) Rybtchinski, B.; Sinks, L. E.; Wasielewski, M. R. *J. Am. Chem. Soc.* **2004**, *126*, 12268–12269.
(44) Abdalla, M. A.; Bayer, J.; Radler, J. O.; Müllen, K. *Angew. Chem., Int. Ed.* **2004**, *43*, 3967–3970.
(45) Bevers, S.; O'Dea, T. P.; McLaughlin, L. W. *J. Am. Chem. Soc.* **1998**, *120*, 11004–11005.
(46) Bevers, S.; Schutte, S.; McLaughlin, L. W. *J. Am. Chem. Soc.* **2000**, *122*, 5905–5915.
(47) Rahe, N.; Rinn, C.; Carell, T. *Chem. Commun.* **2003**, 2120–2121.
(48) Wang, W.; Wan, W.; Zhou, H.-H.; Niu, S.; Li, A. D. Q. *J. Am. Chem. Soc.* **2003**, *125*, 5248–5249.
(49) Zheng, Y.; Long, H.; Schatz, G. C.; Lewis, F. D. *Chem. Commun.* **2005**, 4795–4797.
(50) Zheng, Y.; Long, H.; Schatz, G. C.; Lewis, F. D. *Chem. Commun.* **2006**, 3830–3832.
(51) Bouquin, N.; Malinovskii, V. L.; Haener, R. *Chem. Commun.* **2008**, 1974–1976.
(52) Wagner, C.; Wagenknecht, H. A. *Org. Lett.* **2006**, *8*, 4191–4194.

poly(T)−poly(A) stems containing P located opposite an abasic site and zero, one, or two G−C base pairs. Conjugates **T12** and **A12**, which possess a single P in the middle of a poly(T) or poly(A) 12-mer sequence (Chart 1) have also been investigated. The fluorescence of P is strongly quenched at room temperature in **A12** and all of the hairpins but not in **T12**. Fluorescence quenching occurs via hole injection into either the 3′- or 5′-A adjacent to P, except in the case of **1G**, for which excitation of P leads directly to the radical ion pair (RP) $G^{+\bullet}-P^{-\bullet}$. Rate constants for hole injection, hole transport to G, and charge recombination were obtained from an analysis of femtosecond transient absorption spectra, while the nature of the photogenerated RPs and their spin dynamics were examined by time-resolved EPR (TREPR) spectroscopy.

Experimental Section

Materials. The DNA building block P was prepared and incorporated into oligonucleotide conjugates following the method of Wagner and Wagenknecht.[52] Conjugates were purified by HPLC and characterized by MALDI−TOF mass spectrometry (Table S1 in the Supporting Information). UV−vis absorption measurements were made on a Shimadzu UV1601 spectrometer. Fluorescence spectra were obtained using a Spex Fluoromax spectrofluorimeter. Solutions of the appropriate P−hairpin conjugates in TE buffer (0.02 M Tris, 0.002 M EDTA, pH 7.4) and NaCl (0.1 M) were annealed at 100 °C for 5 min. For low-temperature fluorescence measurements, the solution was further diluted with ethylene glycol to a final concentration of 5 μM. The final solutions containing 30% ethylene glycol, TE buffer, and 0.1 M NaCl were transferred to quartz tubes (3.8 mm OD, 2.4 mm ID), which were submerged in liquid nitrogen contained in an optical hanging-finger Dewar. Samples were excited at $\lambda_{ex} = 505$ nm, and the emission spectra were recorded from 520 to 800 nm. Fluorescence quantum yields were determined using 505 nm excitation by comparing the fluorescence intensity at the emission maximum with that for quinine sulfate solution.[53]

Transient Absorption Spectroscopy. Femtosecond measurements were made using a Ti:sapphire laser system.[42] The instrument response function (IRF) for the pump−probe experiments was 180 fs. Typically, 5 s of averaging was used to obtain the transient spectrum at a given delay time. Solutions of conjugates in TE buffer and 0.1 M NaCl were prepared in cuvettes having a 2 mm path length and irradiated with 505 nm, 130 fs, 0.1−1.0 μJ pulses focused to a spot with a diameter of 200 μm. The optical density at λ_{ex} was between 0.2−0.4. Laser scatter at 505 nm was subtracted from the transient spectra. Analysis of the kinetic data was performed at multiple wavelengths using a Levenberg−Marquardt nonlinear least-squares fit to a general sum-of-exponentials function with an added Gaussian to account for the finite instrument response.

Fluorescence Lifetimes. Fluorescence lifetime measurements were performed using a frequency-doubled, cavity-dumped Ti: sapphire laser as the excitation source and a Hamamatsu C4780 ps fluorescence lifetime measurement system, as described previously.[54] The energy of the 400 nm, 25 fs pulses was attenuated to ∼1.0 nJ/pulse in all of the fluorescence lifetime experiments. The total IRF of the streak camera system was 20 ps. The samples were prepared in 1 cm path length quartz cuvettes, and time-resolved data were collected for each sample at the same concentrations as for the steady-state data. All of the fluorescence data were acquired in single-photon counting mode using the Hamamatsu HPD-TA software. The data was fit using the Hamamatsu fitting module and deconvoluted using the laser-pulse profile.

EPR Spectroscopy. DNA samples for EPR measurements were prepared in the following way: 0.8 mM DNA sample plus 20% glycerol in TE buffer (pH 7.4) was loaded into quartz tubes (3.8 mm OD, 2.4 mm ID) and subjected to several freeze−pump−thaw degassing cycles on a vacuum line (10^{-4} Torr). The tubes were then sealed with a hydrogen torch. TREPR measurements using continuous wave (CW) microwaves and direct detection were made using a Bruker Elexsys E580 X-Band EPR spectrometer outfitted with a variable-Q dielectric resonator (ER-4118X-MD5-W1). The temperature was controlled by an Oxford Instruments CF935 continuous-flow cryostat using liquid N_2. Samples were photoexcited at 532 nm (1−2 mJ/pulse, 7 ns, 10 Hz) using the frequency-doubled output from a Nd:YAG laser (QuantaRay DCR-2). The polarization of the laser was set to 54.7° relative to the direction of the static magnetic field in order to avoid magnetophotoselection effects on the spectra. Following photoexcitation, kinetic traces of transient magnetization were accumulated under CW microwave irradiation (typically 6−20 mW). The field modulation was disabled in order to achieve a time response of $Q/\pi\nu \approx 30$ ns, where Q is the quality factor of the resonator and ν is the resonant frequency, while microwave signals in emission (e) and/or enhanced absorption (a) were detected in both the real and imaginary channels (quadrature detection). Sweeping the magnetic field gave 2D spectra versus both time and magnetic field. For each kinetic trace, the signal acquired prior to the laser pulse was subtracted from the data. Kinetic traces recorded at off-resonance magnetic field values were considered to be background signals, and their average was subtracted from all of the kinetic traces. The spectra were subsequently phased into a Lorentzian part and a dispersive part, and the former, also known as the imaginary magnetic susceptibility χ'', is presented. Simulation of the powder-pattern spectra of the spin-polarized RP signals[55] and the triplet states[56,57] resulting from charge recombination was performed using a home-written MATLAB program[58] following published procedures.

Density Functional Theory Calculations. A calculation on a model adenine radical cation was run using Gaussian 98 software.[59] The geometry of the cation was optimized with density functional theory (DFT) using the B3LYP functional and a 6-31G* basis set. The isotropic hyperfine coupling constants were further optimized with a single-point calculation using the EPR-II basis set (Table S3 in the Supporting Information).

Results

Synthesis and Steady-State Spectra. Oligonucleotides containing the P base-pair surrogate were synthesized by the method of Wagner and Wagenknecht.[52] The CCA linker in hairpins **0G−7G** has been employed previously in the synthesis of stable minihairpins.[60,61] Thermal dissociation profiles provided melting temperatures (T_M) that were ∼10 °C higher than those of corresponding hairpins having an A−T base pair instead of P (Table S2 and Figure S1 in the Supporting Information). Thus, the P base-pair surrogate enhances the thermal stability of these conjugates.

The UV−vis spectra of the P-containing conjugates display characteristic absorption bands of the P monomer having a well-

(53) Kuhn, H. J.; Braslavsky, S. E.; Schmidt, R. *Pure Appl. Chem.* **2004**, *76*, 2105–2146.
(54) Dance, Z. E. X.; Mi, Q. X.; McCamant, D. W.; Ahrens, M. J.; Ratner, M. A.; Wasielewski, M. R. *J. Phys. Chem. B* **2006**, *110*, 25163–25173.
(55) Till, U.; Hore, P. J. *Mol. Phys.* **1997**, *90*, 289–296.
(56) Kottis, P.; Lefebvre, R. *J. Chem. Phys.* **1963**, *39*, 393–403.
(57) Wasserman, E.; Snyder, L. C.; Yager, W. A. *J. Chem. Phys.* **1964**, *41*, 1763–1772.
(58) MATLAB; The MathWorks, Inc.: Natick, MA, 2006.
(59) Frisch, M. J.; et al. Gaussian 98, revision A.97; Gaussian, Inc.: Pittsburgh, PA, 1998.
(60) Yoshizawa, S.; Kawai, G.; Watanabe, K.; Miura, K.; Hirao, I. *Biochemistry* **1997**, *36*, 4761–4767.
(61) Lewis, F. D.; Zhang, L.; Liu, X.; Zuo, X.; Tiede, D. M.; Long, H.; Schatz, G. S. *J. Am. Chem. Soc.* **2005**, *127*, 14445–14453.

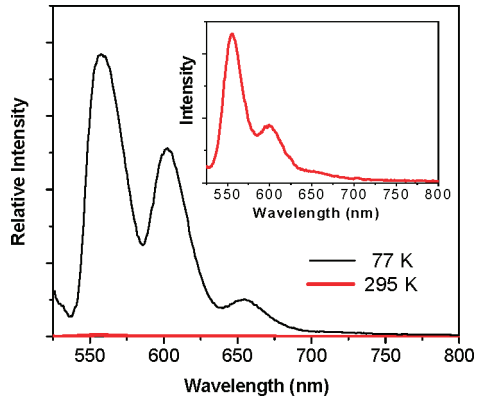

Figure 1. Fluorescence spectra of hairpin **0G** in 30% ethylene glycol, TE Buffer, and 0.1 M NaCl at 77 K (black line) and 295 K (red line). Inset: 295 K spectrum × 100.

defined vibronic ratio of $A^{0-0}/A^{0-1} \approx 1.4$.[62] The CD spectra of hairpins **0G**−**7G** display maxima and minima at short wavelengths (200−300 nm) characteristic of B-form DNA having poly(A) domains.[61,63] The band shifting and inversion in the A^{0-0}/A^{0-1} vibronic ratio characteristic of exciton coupling of the lowest-energy transition of the P chromophores is absent.[49,50] The fluorescence spectra of **0G** (Figure 1) and the other conjugates are mirror images of the P absorption spectra, indicating that the excited state is localized on the P chromophore. Fluorescence quantum yields (Φ_{fluor}) measured at room temperature and 77 K in an ethylene glycol/buffer mixed solvent are reported in Table S2 in the Supporting Information. Hairpins **0G**−**7G** and **A12** are very weakly fluorescent at room temperature ($\Phi_{fluor} < 10^{-3}$); however, **T12** is strongly fluorescent ($\Phi_{fluor} = 0.15$). The fluorescence quantum yields for the hairpins are substantially larger at 77 K ($\Phi_{fluor} = 0.24-0.32$ for **2G**−**5G**), except in the case of **1G** ($\Phi_{fluor} = 0.07$) (Table S2). The fluorescence lifetime of *N*-(2,3-dihydroxypropyl)-P is 2.7 ns, while those of **T12**, **A12**, **0G**, and **7G** are given in footnote [b] of Table 1.

Transient Absorption Spectroscopy. Femtosecond time-resolved transient absorption spectra of the conjugates in aqueous buffer solution were obtained using 505 nm, 130 fs laser pulses. The UV−vis spectra of the samples were recorded prior to and following laser excitation in order to confirm their stability under the conditions of the transient absorption experiments. Transient absorption spectra for **T12**, **0G**, **1G**, and **3G** are shown in Figure 2, and spectra for P and the other conjugates are presented in Figure S2 in the Supporting Information.

Following excitation, the transient spectra of all of the conjugates display positive absorption bands having maxima in the range 707−721 nm and negative bands (bleaches) near 500, 550, and 600 nm (Figure 2 and Figure S2 in the Supporting Information). The negative bands near 500 and 600 nm are assigned to the ground-state depopulation of P and ^{1*}P stimulated emission, respectively, while the negative band near 550 nm is assigned to overlapping ground-state depopulation and stimulated emission.[64] The positive band for **T12** at 707 nm is assigned to absorption of ^{1*}P, whereas the positive bands of all of the other conjugates are assigned to overlapping bands of both ^{1*}P and $P^{-\bullet}$.[42] Single-wavelength kinetics determined at the 605 nm stimulated-emission feature and at 707 and 721 nm within the positive absorption band are reported in Table 1. The single-wavelength kinetics for **T12** determined at these wavelengths are biexponential (Figure 2a, inset), with the major components of both the 605 nm stimulated emission and the 707 nm absorption having decay times of ∼2 ns. The minor decay component of ^{1*}P is most likely indicative of conformational heterogeneity in single-stranded **T12**. The transient spectra of P in CH_2Cl_2 solution (Figure S2a in the Supporting Information) are similar to those for **T12** but have monoexponential decays at 605 and 707 nm.

For **A12** and **0G**−**7G**, the decay of ^{1*}P monitored at 605 nm is biexponential, with one component (τ_{D1}^{605}) having a value less than ∼5 ps while the other component (τ_{D2}^{605}) varies between ∼12−32 ps. Both components have substantial amplitudes and are much shorter than those of **T12**. These short ^{1*}P decay times combined with the very low fluorescence yields for these conjugates (<0.001, Table S2 in the Supporting Information) suggest that photoinduced electron transfer occurs with a quantum yield near unity following formation of ^{1*}P within **A12** and **0G**−**7G**. The τ_{D1}^{605} component is assigned to hole injection into either the 3′ or 5′ A-tract adjacent to ^{1*}P in **A12** and in **0G**, **5G**, and **7G** to give $(A_3)^{+\bullet}-P^{-\bullet}-(A_n)$ or $(A_3)-P^{-\bullet}-(A_n)^{+\bullet}$, respectively. Conjugates **A12** and **0G** contain no G nucleobases, while the G bases in **5G** and **7G** are far enough removed from ^{1*}P that hole trapping by G is inefficient relative to charge recombination. As will be discussed below, charge recombination of either $(A_3)^{+\bullet}-P^{-\bullet}-(A_n)$ or $(A_3)-P^{-\bullet}-(A_n)^{+\bullet}$ results in repopulation of ^{1*}P, yielding delayed fluorescence that is monitored as the longer stimulated-emission decay component, τ_{D2}^{605}. The values of τ_{D2}^{605} for **A12**, **0G**, and **7G** agree well with their fluorescence lifetimes, given the 20 ps instrument response of the time-resolved fluorescence apparatus (footnote [b] of Table 1). The positive absorption bands of **A12**, **0G**, **5G**, and **7G** are broader than that of **T12**, starting at ∼630 nm and extending beyond the 810 nm long-wavelength cutoff of the spectral window. These bands in **A12**, **0G**, **5G**, and **7G** are dominated by the absorption of $P^{-\bullet}$, as evidenced by their monoexponential decay times τ_{D1}^{707} and τ_{D1}^{721}.

The transient absorption band of **1G** (Figure 2c) exhibits a rapid time-dependent red shift from 707 to 721 nm and is less symmetric than that of **0G**. The 721 nm transient is assigned to the $G^{+\bullet}-P^{-\bullet}$ contact RP because G is much easier to oxidize than A.[65] The 605 nm stimulated-emission band assigned to ^{1*}P is much weaker than that of **0G**. The decay times τ_{D1}^{707} and τ_{D1}^{721} are both ∼1.0 ps and are attributed to charge recombination of the $G^{+\bullet}-P^{-\bullet}$ contact RP (Figure 2c, inset).

The transient spectra of **2G**−**4G** (Figure 2d and Figure S2c,d in the Supporting Information) are similar in appearance to that of **1G** but have stronger 600 nm stimulated-emission bands and display slower time-dependent shifts in their absorption bands from 707 to 721 nm. The decays of these bands are biexponential, with each hairpin having one decay component (τ_{D1}^{707} and τ_{D1}^{721}) comparable to the long stimulated-emission component τ_{D2}^{605} and a second decay component (τ_{D2}^{707} and τ_{D2}^{721}) that depends on the location of G, with the decay time increasing as the distance between P and G increases (Table 1). The τ_{D1}^{707} and τ_{D1}^{721} components are attributed to charge recombination of

(62) Li, A. D. Q.; Wang, W.; Wang, L.-Q. *Chem.−Eur. J.* **2003**, *9*, 4594–4601.
(63) Gudibande, S. R.; Jayasena, S. D.; Behe, M. J. *Biopolymers* **1988**, *27*, 1905–1915.
(64) Giaimo, J. M.; Lockard, J. V.; Sinks, L. E.; Vega, A. M.; Wilson, T. M.; Wasielewski, M. R. *J. Phys. Chem. A* **2008**, *112*, 2322–2330.
(65) Seidel, C. A. M.; Schulz, A.; Sauer, M. H. M. *J. Phys. Chem.* **1996**, *100*, 5541–5553.

Table 1. Transient Absorption Kinetics for Perylenediimide DNA Conjugates[a]

conjugate	τ_{D1}^{605}(ps)	τ_{D2}^{605} (ps)	τ_{D1}^{707} (ps)	τ_{D2}^{707} (ps)	τ_{D1}^{721} (ps)	τ_{D2}^{721} (ps)
T12	96 ± 3 (0.18)	2100 ± 200[b] (0.82)	116 ± 5 (0.20)	1800 ± 200 (0.80)	–	–
A12	2.0 ± 0.1 (0.63)	11.1 ± 0.2[b] (0.37)	11.4 ± 0.2	–	–	–
0G	4.2 ± 0.4 (0.48)	29 ± 2[b] (0.52)	35.6 ± 0.3	–	35.5 ± 0.3	–
1G	0.3 ± 0.1	–[c]	1.0 ± 0.1	–	1.0 ± 0.1	–
2G	2.2 ± 0.1 (0.60)	11.8 ± 0.5 (0.40)	11.2 ± 0.1 (0.90)	31.9 ± 0.4 (0.10)	11.1 ± 0.1 (0.87)	32.5 ± 0.4 (0.13)
3G	3.5 ± 0.1 (0.34)	21.2 ± 0.4 (0.66)	24.2 ± 0.2 (0.63)	103 ± 3 (0.37)	31 ± 1 (0.73)	126 ± 12 (0.27)
4G	3.9 ± 0.1 (0.43)	28.0 ± 0.4 (0.57)	30 ± 1 (0.93)	>3000 (0.07)	33 ± 1 (0.89)	>3000 (0.11)
5G	4.3 ± 0.1 (0.43)	31 ± 2 (0.57)	34.1 ± 0.4	–	35.6 ± 0.4	–
7G	5.1 ± 0.2 (0.44)	31.6 ± 0.6[b] (0.56)	35.5 ± 0.4	–	34.4 ± 0.9	–

[a] The superscripts of the column headings indicate the emission wavelengths; amplitudes of the exponential kinetic components are shown in parentheses. [b] The monoexponential fluorescence decay times are 2.5 ± 0.1 ns for **T12**, <20 ps for **A12**,; 32 ± 1 ps for **0G**, and 34 ± 1 ps for **7G**. [c] The small-amplitude positive absorption observed at 605 nm following decay of the stimulated emission decays with a lifetime of τ = 1.3 ± 0.2 ps.

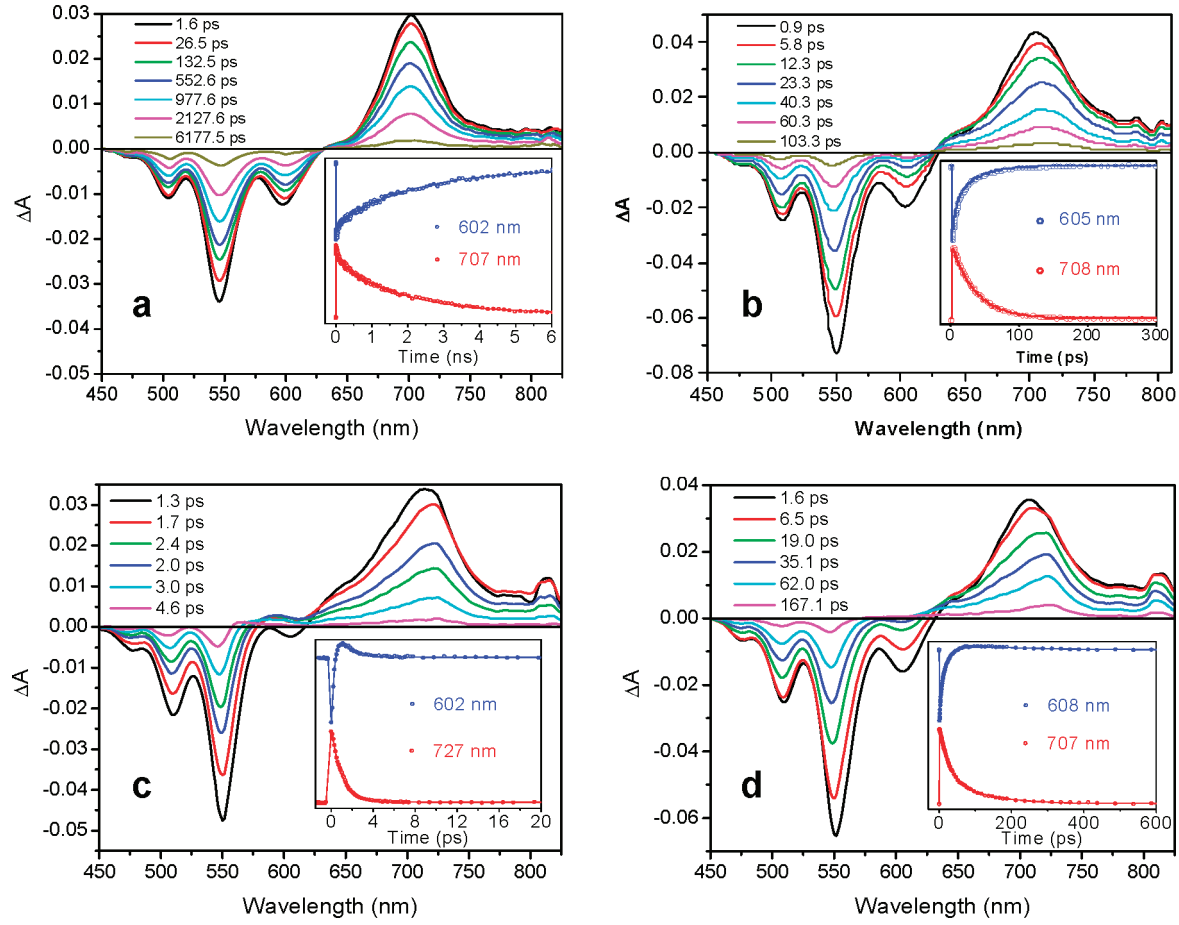

Figure 2. Transient absorption spectra of hairpins (a) **T12**, (b) **0G**, (c) **1G**, and (d) **3G** in TE buffer following excitation with 505 nm, 130 fs laser pulses. Insets: transient absorption kinetics at the indicated wavelengths. Nonlinear least-squares fits to the data are also shown.

$(A_3)^{+\bullet}-P^{-\bullet}-(A_n)$ or $(A_3)-P^{-\bullet}-(A_n)^{+\bullet}$ and the $\tau_{D2}^{707}$and τ_{D2}^{721}components to charge recombination of $(A_3)-P^{-\bullet}-(A_n)-G^{+\bullet}$ formed upon hole transport from $(A_n)^{+\bullet}$ to G.

Radical-Pair TREPR Spectra. TREPR measurements were used to probe the mechanism of charge recombination within the hairpins and the electronic interactions between the two radical ions. Following rapid charge separation, the initially formed singlet RP $^1(D^{+\bullet}-P^{-\bullet})$, where D is A or G, undergoes radical-pair intersystem crossing (RP-ISC)[66,67] to produce the triplet RP $^3(D^{+\bullet}-P^{-\bullet})$ (Figure 3A). TREPR measurements were carried out in a 350 mT magnetic field to ensure that the triplet sublevels of $^3(D^{+\bullet}-P^{-\bullet})$ undergo Zeeman splitting (Figure 3B) and are best described by the T_{+1}, T_0, and T_{-1} eigenstates that are quantized along the applied magnetic field.[54,68−70] RP-ISC depends on both the spin−spin exchange interaction, 2*J*, and the dipolar interaction, *D*, between the two radicals that comprise

(66) Closs, G. L.; Forbes, M. D. E.; James, R.; Norris, J. *J. Phys. Chem.* **1987**, *91*, 3592–3599.
(67) Hore, P. J.; Hunter, D. A.; McKie, C. D.; Hoff, A. J. *Chem. Phys. Lett.* **1987**, *137*, 495–500.
(68) Hasharoni, K.; Levanon, H.; Greenfield, S. R.; Gosztola, D. J.; Svec, W. A.; Wasielewski, M. R. *J. Am. Chem. Soc.* **1996**, *118*, 10228–10235.
(69) Carbonera, D.; DiValentin, M.; Corvaja, C.; Agostini, G.; Giacometti, G.; Liddell, P. A.; Kuciauskas, D.; Moore, A. L.; Moore, T. A.; Gust, D. *J. Am. Chem. Soc.* **1998**, *120*, 4398–4405.
(70) Kobori, Y.; Yamauchi, S.; Akiyama, K.; Tero-Kubota, S.; Imahori, H.; Fukuzumi, S.; Norris, J. R., Jr. *Proc. Natl. Acad. Sci. U.S.A.* **2005**, *102*, 10017–10022.

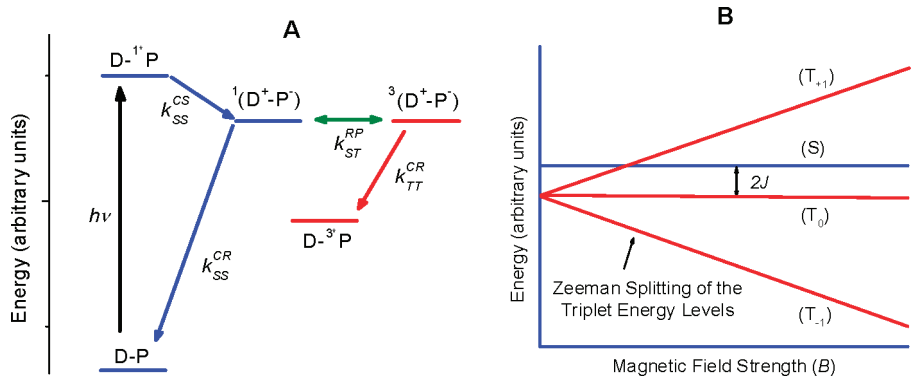

Figure 3. (A) Electron-transfer and intersystem-crossing pathways in a D−B−A system. (B) RP energy levels as a function of magnetic field for $2J > 0$ and $D = 0$.

the RP. The magnitude of $2J$ depends exponentially on the distance r between the two radicals and is assumed to be isotropic, while that of D depends on $1/r^3$ and is anisotropic. For large molecules in solution, such as the hairpins studied here, and for molecules in the solid state, D is not rotationally averaged to zero. D is usually approximated by the point-dipole model as[71]

$$D = -\frac{3\mu_0 g_e^2 \beta_e^2}{8\pi r^3} \quad (1)$$

where μ_0, g_e, and β_e are the vacuum permeability, electronic g-factor, and Bohr magneton, respectively. For D in milliteslas and r in angstroms, $D = -(2785\ \text{mT Å})/r^3$. For RP distances greater than ∼10−15 Å, both D and $2J$ are small; in this case, the S and T_0 spin states of the RP are close in energy and mix, while the T_{+1} and T_{-1} states are energetically far-removed from T_0 and do not mix with S.[54,68–70] The two RP states that result from S−T_0 mixing are preferentially populated as a result of the initial population of S, so the four $\Delta m = \pm 1$ EPR transitions that occur between these two mixed states and T_{+1} and T_{-1} display an intensity pattern characteristic of the strong spin polarization.[66,67] The TREPR spectrum consists of two antiphase doublets centered at the g-factors of the individual radicals that comprise the pair, in which the splitting of each doublet is determined by $2J$ and D. The electron-spin-polarization pattern of the EPR signal, i.e., the pattern of a and e transitions in going from low field to high field, is determined by the sign rule:[54,72]

$$\Gamma = \mu\ \text{sign}(2J - D) = \begin{cases} - & \text{for } (e, a) \\ + & \text{for } (a, e) \end{cases} \quad (2)$$

where μ is -1 or $+1$ for a singlet or triplet excited-state precursor, respectively. Since ultrafast charge separation in the hairpins proceeds from ^{1*}P and the resultant RP spectra exhibit an (e, a) spin-polarization pattern, eq 2 restricts the signs and magnitudes that $2J$ and D can adopt. Given that D is negative (eq 1), if $2J > 0$, eq 2 predicts an (e, a) pattern for all values of $2J$ and D, while if $2J < 0$, eq 2 predicts an (e, a) pattern only when $|D| > |2J|$.[66,67]

Following excitation with a 532 nm, 7 ns laser pulse, spin-polarized RP signals were observed by TREPR for both **0G** and **4G** at 85 K and for **4G** at 295 K (Figure 4). Since the g-factors of the two radicals are similar, significant overlap of the two antiphase doublets results in one dominant doublet

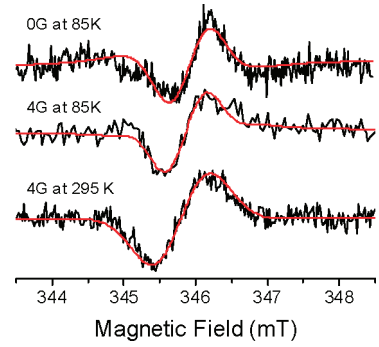

Figure 4. TREPR spectra of **0G** and **4G** at 85 K and **4G** at 295 K recorded 100 ns after a 532 nm, 7 ns, 2.5 mJ laser pulse. The smooth curves superimposed on the experimental spectra are computer simulations of the RP spectra using the parameters given in Table 2.

having an (e, a) spin-polarization pattern. The spectra were simulated using the spin-correlated radical-pair model,[55,66,67,73,74] and the hyperfine coupling constants were calculated for $A^{+\bullet}$ using DFT (see the Experimental Section) and measured for $G^{+\bullet}$ [75] and $PDI^{-\bullet}$.[76] The model accounts for the spin-selective rates of decay by charge recombination for the singlet and triplet RPs (k_{SS}^{CR} and k_{TT}^{CR}, respectively, in Figure 3A).[55] The fits to the data are shown in Figure 4, and the values of the parameters obtained from the fits are summarized in Table 2. The parameter $\tau_{SSTT} = 2/(k_{SS}^{CR} + k_{TT}^{CR})$ is the overall time constant for RP decay predicted by fitting the TREPR spectra,[55] while τ_{CR} is the RP-decay time constant monitored at the magnetic field of the enhanced-absorption peak in the TREPR spectra. The values of τ_{SSTT} and τ_{CR} agree reasonably well, given the modest signal-to-noise ratio in the observed TREPR spectra. The distances between the two radicals in the RPs were determined using D values obtained from the simulations and eq 1 (Table 2). The lifetime of $(A_n)^{+\bullet}-P^{-\bullet}$ in **0G** is too short to observe by TREPR at 295 K, but interestingly, a spin-correlated RP signal is readily observed at 85 K and gives a D value consistent with trapping of the hole at the same distance from $P^{-\bullet}$ as observed for **4G**.

Spectra of Triplet States Resulting from Charge Recombination. The subsequent charge-recombination process is spin-selective, i.e., $^1(D^{+\bullet}-P^{-\bullet})$ recombines to form the singlet ground

(71) Efimova, O.; Hore, P. J. *Biophys. J.* **2008**, *94*, 1565–1574.
(72) Hore, P. J. In *Advanced EPR in Biology and Biochemistry*; Hoff, A. J., Ed.; Elsevier: Amsterdam, 1989; pp 405−440.
(73) Buckley, C. D.; Hunter, D. A.; Hore, P. J.; McLauchlan, K. A. *Chem. Phys. Lett.* **1987**, *135*, 307–312.
(74) Norris, J. R.; Morris, A. L.; Thurnauer, M. C.; Tang, J. *J. Chem. Phys.* **1990**, *92*, 4239–4249.
(75) Huttermann, J.; Voit, K.; Oloff, H.; Kohnlein, W.; Graslund, A.; Rupprecht, A. *Faraday Discuss.* **1984**, 135–149.
(76) Tauber, M. J.; Kelley, R. F.; Giaimo, J. M.; Rybtchinski, B.; Wasielewski, M. R. *J. Am. Chem. Soc.* **2006**, *128*, 1782–1783.

Table 2. Charge-Recombination Times and Simulation Parameters for RP Spectra of **0G** and **4G** Measured by TREPR 100 ns after the Laser Pulse

conjugate	T (K)	$2J$ (mT)	D (mT)	r (Å)	k_{SS}^{CR} (10^6 s^{-1})	k_{TT}^{CR} (10^6 s^{-1})	τ_{SSTT} (ns)	τ_{CR} (ns)
0G	85	0.01 ± 0.02	-1.1 ± 0.1	13.6 ± 0.5	6 ± 1	13 ± 1	105 ± 12	166 ± 60
4G	295	0.08 ± 0.02	-0.9 ± 0.1	14.6 ± 0.5	12 ± 1	17 ± 1	68 ± 6	51 ± 3
4G	85	0.06 ± 0.02	-1.1 ± 0.1	13.6 ± 0.5	7 ± 1	12 ± 1	105 ± 12	99 ± 10

state while $^3(D^{+\bullet}-P^{-\bullet})$ recombines to yield the triplet $D-^{3*}P$, which acquires the non-Boltzmann spin population of the triplet RP state.[77] The spin polarization of the EPR transitions exhibited by $D-^{3*}P$ can be differentiated from those of a triplet state formed by the ordinary spin−orbit intersystem-crossing mechanism on the basis of the polarization pattern of its six EPR transitions at the canonical (x, y, z) orientations relative to the applied magnetic field. An RP precursor that undergoes the RP-ISC mechanism by $S-T_0$ mixing followed by charge recombination uniquely yields an (a, e, e, a, a, e) spin-polarization pattern.[77]

The TREPR spectra of **0G** and **4G** were recorded at 85 K. A very weak triplet spectrum was observed for **4G** (Figure 5), while no triplet spectrum was observed for **0G**. The triplet spectrum of **4G** is broad, with a width of ~98 mT, and has a spin-polarization pattern of (a, e, e, a, a, e), which is the unique signature for the RP-ISC mechanism. In comparison, PDI chromophores have intrinsically high fluorescence quantum yields, so their triplet yields due to spin−orbit-induced intersystem crossing are very small.[54] The narrow signal at the center of the spectrum ($g \approx 2$) is produced by the RP discussed above. The triplet spectral line shape was simulated using the RP-ISC mechanism, yielding zero-field splitting values of $D = 46$ mT and $E = -4.8$ mT. These measured values of the zero-field splittings for the triplet state agree well with those observed previously for ^{3*}PDI derivatives.[54]

Discussion

Charge-Transfer Energetics. Previous studies of DNA−PDI and P conjugates have provided only qualitative evidence for fluorescence quenching of PDI fluorescence by covalently attached nucleobases.[46,52] The PDI chromophore is a strong photochemical oxidant and has been widely employed in studies of photoinduced electron transfer.[14–19,21,23,40–43,78] The free energies of charge separation and charge recombination (ΔG_{CS} and ΔG_{CR}, respectively) were estimated using Weller's expression[79] (based on the Born dielectric-continuum model of the solvent) for the free energy of formation of an ion pair, ΔG_{IP}, in a solvent of arbitrary polarity:

$$\Delta G_{IP} = E_{OX} - E_{RED} - \frac{e^2}{r_{DA}\varepsilon_S} + e^2\left(\frac{1}{2r_1} + \frac{1}{2r_2}\right)\left(\frac{1}{\varepsilon_S} - \frac{1}{\varepsilon_{SP}}\right) \quad (3)$$

$$\Delta G_{CS} = \Delta G_{IP} - E_S \quad (4)$$

$$\Delta G_{CR} = -\Delta G_{IP} \quad (5)$$

where E_{OX} is the nucleobase oxidation potential (1.24 V for G, 1.69 V for A, and ~1.9 V for T or C vs SCE in acetonitrile)[65] and E_{RED} is the reduction potential of P (−0.43 V vs SCE in DMF)[80] measured in a solvent having dielectric constant ε_{SP} (in this case, $\varepsilon_{SP} = 38$ for both CH_3CN and DMF), e is the charge of an electron, r_1 and r_2 are the effective ionic radii of the radical ions, r_{DA} is the donor−acceptor distance, ε_S is the static dielectric constant of the solvent in which the spectroscopy is performed, and E_S is the energy of ^{1*}P (2.26 eV). If a moderately polar environment for the interior of DNA ($\varepsilon_S \approx 10$) is assumed,[81,82] oxidation of nucleobase donors adjacent to ^{1*}P, where $r_{DA} \approx 3.5$ Å and the effective ionic radii r_1 and r_2 are both equal to $r_{DA}/2$, should be highly exergonic for G, approximately isoergonic for A, and endergonic for T and C. This is consistent with the observation of efficient quenching of P fluorescence at 295 K for **A12** and all of the hairpins ($\Phi_{fluor} < 10^{-3}$) but not for **T12** ($\Phi_{fluor} = 0.15$).

Fluorescence quenching in the hairpins is much less efficient at 77 K in a rigid glass than at room temperature in a fluid solution, with values of Φ_{fluor} increasing to 0.07 for **1G** and 0.24−0.32 for **2G**−**5G** (Table S2 in the Supporting Information). Decreased quenching is consistent with destabilization of RPs in rigid glasses versus polar liquids.[83] The consequent decrease in ΔG_{CS} would reduce the rate of charge separation, which is consistent with the increase in fluorescence yield.

Hole Injection. The mechanism used to analyze the kinetic data for both charge separation and charge recombination in conjugates **0G** and **2G**−**7G** is shown in Scheme 1A, while that for **1G** is shown in Scheme 1B. Following photoexcitation of P in **0G** and **2G**−**7G**, hole injection to the adjacent A bases in either the 3′ or 5′ direction can occur, while in **1G**, the 5′ side of P has an adjacent G.[84] Given that $(A_3)^{+\bullet}-P^{-\bullet}-(A_n)-G$ and $(A_3)-P^{-\bullet}-(A_n)^{+\bullet}-G$ are nearly isoenergetic with ^{1*}P, the initial formation of these RPs (k_{CS1} and k_{CS2}) in **2G**−**7G** may be followed by charge recombination that repopulates ^{1*}P (k_{CR1} and k_{CR2}), resulting in its observed biexponential stimulated emission, or by competitive charge recombination to the ground state (k_{CR3} and k_{CR4}) and hole transport to G (k_{CS3}). Trapping of the hole at G forms $(A_3)-P^{-\bullet}-(A_n)-G^{+\bullet}$, which is ~0.4 eV more stable than either $(A_3)^{+\bullet}-P^{-\bullet}-(A_n)-G$ or $(A_3)-P^{-\bullet}-(A_n)^{+\bullet}-G$, and thus, $(A_3)-P^{-\bullet}-(A_n)-G^{+\bullet}$ recombines to the ground state (k_{CR5}). The role of spin-selective recombination to form ^{3*}P is discussed below.

The transient decay kinetics of the stimulated emission from **0G**, **5G**, and **7G** at 605 nm are biexponential, whereas those of the absorptions at both 707 and 721 nm, where ^{1*}P and $P^{-\bullet}$ strongly overlap, are monoexponential. Because of this significant spectral overlap and the appearance of the 707 and 721 nm absorption features in <5 ps, an accurate analysis of their rise kinetics could not be made within the quality of the data.

(77) Levanon, H.; Hasharoni, K. *Prog. React. Kinet.* **1995**, *20*, 309–346.
(78) Ahrens, M. J.; Kelley, R. F.; Dance, Z. E. X.; Wasielewski, M. R. *Phys. Chem. Chem. Phys.* **2007**, *9*, 1469–1478.
(79) Weller, A. *Z. Phys. Chem.* **1982**, *133*, 93–98.
(80) Gosztola, D.; Niemczyk, M. P.; Svec, W. A.; Lukas, A. S.; Wasielewski, M. R. *J. Phys. Chem. A* **2000**, *104*, 6545–6551.
(81) Lewis, F. D.; Liu, X.; Miller, S. E.; Hayes, R. T.; Wasielewski, M. R. *J. Am. Chem. Soc.* **2002**, *124*, 14020–14026.
(82) Tavernier, H. L.; Fayer, M. D. *J. Phys. Chem. B* **2000**, *104*, 11541–11550.
(83) Gaines, G. L.; O'Neil, M. P.; Svec, W. A.; Niemczyk, M. P.; Wasielewski, M. R. *J. Am. Chem. Soc.* **1991**, *113*, 719–721.
(84) Fukui, K.; Tanaka, T. *Angew. Chem., Int. Ed.* **1998**, *37*, 158–161.

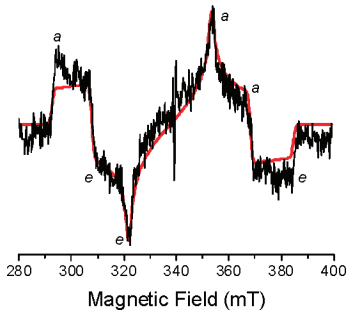

Figure 5. Triplet EPR spectrum of **4G** recorded at 85 K. The labels *a* and e denote enhanced absorption and emission, respectively. The simulation parameters obtained from fitting the spectrum are $D = 46$ mT and $E = -4.8$ mT.

Scheme 1

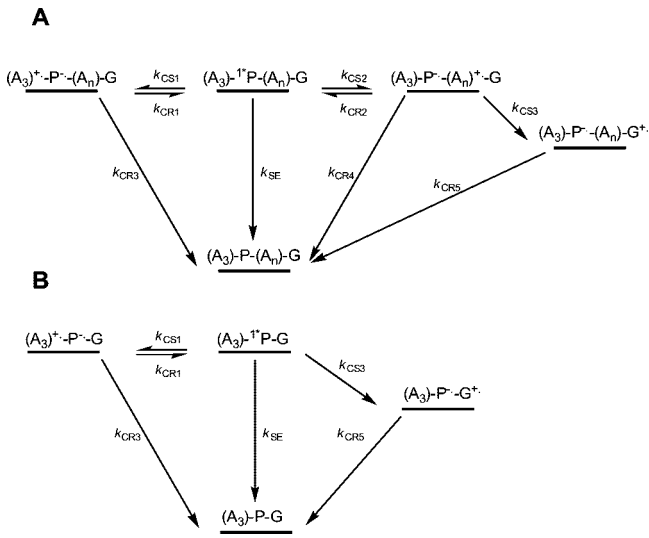

Table 3. Rate Constants (10^{10} s^{-1}) for Charge Separation and Recombination within DNA Conjugates and Selected RP Yields

hairpin	k_{CS1}	k_{CR1}	k_{CS2}	k_{CR2}	k_{CS3}	k_{CR3}	k_{CR4}	k_{CR5}	$\phi(P^{-\bullet}-G^{+\bullet})$
0G	4.5	7.8	4.5	7.8	–	7.0	7.0	–	–
1G	4.5[a]	7.8[a]	–	–	300	7.0[a]	–	100	1.0
2G	4.5[a]	7.8[a]	23	20	15	7.0[a]	7.0	3.1	0.57
3G	4.5[a]	7.8[a]	10	20	10	7.0[a]	7.0	0.79	0.40
4G	4.5[a]	7.8[a]	7.0	14	3.3	7.0[a]	7.0	0.0023	0.19
5G	4.5	7.8	4.5	7.8	–	7.0	7.0	–	<0.05
7G	4.5	7.8	4.5	7.8	–	7.0	7.0	–	<0.05

[a] These rate constant values were fixed at the corresponding value for **0G** in the kinetic simulations.

In view of the absence of G within **0G** and the nearly identical kinetic data for **0G**, **5G**, and **7G** at each wavelength monitored (Table 1), the data strongly suggest that hole transport to G within **5G** and **7G** is not competitive with repopulation of ^{1*}P and charge recombination of $(A_3)-P^{-\bullet}-(A_n)^{+\bullet}-G$. Kinetic simulations[85] of the transient absorption decay data were carried out assuming that $k_{CS1} = k_{CS2} = 1/2\tau_{D1}^{605}$, $k_{CR1} = k_{CR2} = 1/2\tau_{D2}^{605}$, and $k_{CR3} = k_{CR4} \approx 1/\tau_{D1}^{721}$ (or $1/\tau_{D1}^{707}$). The values of the rate constants were varied to fit the kinetic model and the observed amplitudes of τ_{D1}^{605} and τ_{D2}^{605}, and the results are presented in Table 3. Interestingly, the charge separation (hole injection) rates are 1.5−2 times smaller than those for both repopulation of ^{1*}P and charge recombination to the ground state. This ordering of rates is required by the fact that the amplitudes of τ_{D2}^{605} are larger for all of these these conjugates, suggesting that the energy levels of $(A_3)^{+\bullet}-P^{-\bullet}-(A_n)-G$ and $(A_3)-P^{-\bullet}-(A_n)^{+\bullet}-G$ are slightly higher than that of ^{1*}P.

To analyze the data for **1G** (Scheme 1B), the kinetic analysis assumed that the values of k_{CS1}, k_{CR1}, and k_{CR3} for **1G** are the same as those for **0G** and varied the remaining rate constants to fit the transient kinetic data. The stimulated emission decay ($\tau_{D1}^{605} = 0.3$ ps) for **1G** is monoexponential and ~10 times faster than that for the conjugates having only A bases adjacent to ^{1*}P, so charge separation in **1G** is dominated entirely by oxidation of the adjacent G to form the contact RP with a rate constant of $k_{CS3} = 1/\tau_{D1}^{605} = 3 \times 10^{12}$ s^{-1}. Faster charge separation that preferentially yields $(A_3)-P^{-\bullet}-G^{+\bullet}$ rather than $(A_3)^{+\bullet}-P^{-\bullet}-(A_n)-G$ or $(A_3)-P^{-\bullet}-(A_n)^{+\bullet}-G$ is consistent with greater ease of oxidation of G than of A (eqs 3 and 4).[81,86] The $(A_3)-P^{-\bullet}-G^{+\bullet}$ contact ion pair recombines very rapidly, with $k_{CR5} = 1/\tau_{D1}^{721} = 1.0 \times 10^{12}$ s^{-1}.

The transient absorption kinetics for **2G**−**4G** vary in interesting and informative ways as the distance between P and G increases (Table 1). Once again, stimulated emission from **2G**−**4G** at 605 nm is biexponential, with τ_{D1}^{605} and τ_{D2}^{605} both increasing by a factor of ~2 as the P−G distance increases. In addition, the amplitudes of these components show a systematic variation in which the short component dominates at the short P−G distance in **2G** while the long component once again dominates at the longer P−G distance in **4G**. The 707 and 721 nm transient absorption bands also show biexponential decays for **2G**−**4G** in which τ_{D1}^{707} and τ_{D1}^{721} are very similar to τ_{D2}^{605} for stimulated emission. On the other hand, the second, long decay components τ_{D2}^{707} and τ_{D2}^{721} become longer as the G−P distance increases. These decay data were analyzed in the context of the kinetic pathways presented in Scheme 1A. Once again, it was assumed that the charge-transfer kinetics involving $(A_3)^{+\bullet}-P^{-\bullet}-(A_n)-G$ are the same as those measured for **0G** and that the rate constants for charge recombination of $(A_3)^{+\bullet}-P^{-\bullet}-(A_n)-G$ and $(A_3)-P^{-\bullet}-(A_n)^{+\bullet}-G$ to the ground state are the same, i.e., $k_{CR3} = k_{CR4}$. The rate constants k_{CS2}, k_{CR2}, and k_{CS3} involving the $(A_3)-P^{-\bullet}-(A_n)^{+\bullet}-G$ and $(A_3)-P^{-\bullet}-(A_n)-G^{+\bullet}$ intermediates were varied to fit the time constants τ_{D1}^{605}, τ_{D2}^{605}, and τ_{D1}^{721} (or τ_{D1}^{707}), respectively, and their amplitudes, while $k_{CR5} = 1/\tau_{D2}^{721}$ (or $1/\tau_{D2}^{707}$) was used as a starting value in the fits.

The initial charge-separation (hole-injection) rate (k_{CS2}) for the formation of $(A_3)-P^{-\bullet}-(A_n)^{+\bullet}-G$ in **4G** (Table 3) is only about 1.5 times larger than those in **0G**, **5G**, and **7G**, in which no competitive electron transfer to G occurs. This rate increases strongly as the number of A bases between P and G decreases, i.e., for **3G** and **2G**. A similar but weaker trend is observed for the rate of charge recombination of $(A_3)-P^{-\bullet}-(A_n)^{+\bullet}-G$, which repopulates ^{1*}P. The rate constants for the subsequent hole-transfer reaction to G, i.e., $(A_3)-P^{-\bullet}-(A_n)^{+\bullet}-G \rightarrow (A_3)-P^{-\bullet}-(A_n)-G^{+\bullet}$, decrease significantly as the G−P distance increases.

The data suggest that charge separation within **2G**−**4G** occurs primarily by a stepwise process, namely, hole injection by ^{1*}P into the A-tract followed by hole transport to G, analogous to the mechanism for charge separation in capped hairpins having

(85) Chemical Kinetics Simulator, version 1.01; IBM: San Jose, CA, 1996.

(86) Lewis, F. D.; Kalgutkar, R. S.; Wu, Y. S.; Liu, X. Y.; Liu, J. Q.; Hayes, R. T.; Miller, S. E.; Wasielewski, M. R. *J. Am. Chem. Soc.* **2000**, *122*, 12346–12351.

stilbene donor and acceptor chromophores,[81,87] rather than the superexchange process initially proposed for hairpins having a stilbene hole donor and guanine hole acceptor.[88] The simplest model, as originally suggested by Giese and co-workers,[89,90] involves rapid hole injection from ^{1*}P into the A-tract to form the contact RP $P^{-\bullet}-A^{+\bullet}$ followed by discrete hole hopping between adjacent A bases until the charge is trapped by G. It has been noted recently that the Coulomb stabilization is largest for the contact ion pair $P^{-\bullet}-A^{+\bullet}$ and decreases asymptotically as the distance between the charges increases, which may result in a significant dependence of the hole-transport rate on distance.[91] For the series **2G**−**4G**, the rate of hole transport to G (k_{CS3}) decreases by a factor of only 4.5 for a change in distance from 3.5 to 10.5 Å, implying that the Coulomb interaction between the hole residing on the A-tract and $P^{-\bullet}$ is not as large as expected by this model. The soft distance-dependence of k_{CS3} may be a consequence of production of a polaron involving several adjacent A bases via hole injection, so for short A-tracts, as are found in **2G**−**4G**, hole injection into the A-tract leads to a single delocalized radical cation, $(A_n)^{+\bullet}$. Conwell and co-workers[92,93] have advanced a polaron model in which the hole is delocalized over 3−5 adenines, and an ion-gated, polaron-like hole-transport model has been proposed by Schuster and Landman.[94] Renger and Marcus[95] have proposed a delocalized-state model in which the energy splitting between bridge states increases as the bridge becomes longer.

Polaron formation followed by its trapping by G is also consistent with the observed changes in the rate constants for both hole injection (k_{CS2}) and ^{1*}P repopulation (k_{CR2}). In the limit where the polaron is not competitively trapped by G, as in the case of **0G**, **5G**, and **7G**, the polaron achieves the maximum delocalization length allowed by the electronic coupling between the A bases and the Coulomb interaction between $(A_n)^{+\bullet}$ and $P^{-\bullet}$. Since no competitive trapping of the polaron by G is observed for **5G**, for which $n = 4$, the delocalization length of the polaron is no more than 3−4 A bases. As the number of A bases decreases below four, as in the case of **2G**−**4G**, the $(A_n)^{+\bullet}$ polaron is confined to 1−3 A bases, respectively, resulting in a stronger Coulomb interaction between the charges on $(A_n)^{+\bullet}$ and $P^{-\bullet}$ as well as increased electronic-coupling matrix elements for both hole injection and ^{1*}P repopulation, which result in larger rate constants for these processes.

Charge Recombination in Long-Lived RPs. Given that the value of k_{CR5} obtained for **4G** from the transient absorption experiments is much longer (>3 ns) than can be accurately determined from our 0−6 ns delay-time window, we examined the RP prepared upon photoexcitation of P in **4G** using TREPR. The TREPR spectra observed at 295 and 85 K are both characteristic of a spin-correlated RP. The observation of a spin-correlated RP upon irradiation of DNA hairpins possessing a naphthalene-1,8:4,5-bis(dicarboximide) (NI) linker has recently been reported at 30 K but not at room temperature.[96] The RP lifetimes of **4G** at 295 K determined from the spectral fit and direct observation of the RP TREPR decay kinetics are both ∼2 times shorter than those observed at 85 K (Table 2), yet the values of $2J$ and D do not vary with temperature within experimental uncertainty. Since the oxidation potential of G is much lower than that of A, G functions as a deep hole trap in **4G** at room temperature as well as in the glassy solvent at low temperature. The ∼14 Å distance obtained from D for $(A_3)-P^{-\bullet}-(A_3)-G^{+\bullet}$ at both temperatures is consistent with the average spacing of 3.5 Å between the π-stacked base pairs.

No TREPR signals were observed at either 295 or 85 K for **2G**. The transient absorption data show that $k_{CR5} = 3.1 \times 10^{10}$ s^{-1} in **2G**, so it is likely that the lifetime of $(A_3)-P^{-\bullet}-(A_1)-G^{+\bullet}$ at 85 K is also shorter than the ∼30 ns instrument response time of the TREPR experiment, making this species difficult to detect. Interestingly, a spin-correlated RP is observed in **0G** at 85 K but *not* at 295 K. The room-temperature result is consistent with our transient absorption data, which shows that $(A_3)^{+\bullet}-P^{-\bullet}-(A_n)$ and $(A_3)-P^{-\bullet}-(A_n)^{+\bullet}$ recombine with $\tau = 35.5$ ps in **0G**. The D value for **0G** at 85 K is the same as that of **4G**, so the RP distances in both molecules are ∼14 Å, which implies that the hole is trapped on the A base in the fourth A−T base pair away from $P^{-\bullet}$. The changes in **0G** that produce an A-base trap site at 85 K are a matter of speculation, but conformational and/or specific changes to the local solvation environment of the A base relative to the other bases are likely possibilities.

Spin-selective charge recombination of $(A_3)-P^{-\bullet}-(A_3)-G^{+\bullet}$ in **4G** results in the formation of a triplet state that exhibits a spin-polarized TREPR spectrum (Figure 5); however, no triplet TREPR signal is observed for **0G** or **2G**. The relatively weak triplet signal shown in Figure 5 is consistent with the low quantum yield (0.19) of $(A_3)-P^{-\bullet}-(A_3)-G^{+\bullet}$ in **4G**. The values of k_{SS}^{CR} and k_{TT}^{CR} indicate that ∼60% of the RP population decays to produce ^{3*}P, so the overall yield of ^{3*}P is at most 12%. The triplet EPR spectrum for **4G** has the (*a*, *e*, *e*, *a*, *a*, *e*) spin-polarization phase pattern diagnostic of spin-selective charge recombination of a triplet RP precursor formed by the RP-ISC mechanism. The absence of a triplet EPR spectrum from **0G** at 85 K most likely reflects an even lower yield of $(A_3)-P^{-\bullet}-(A_3)-A^{+\bullet}$, as evidenced by the poorer signal-to-noise ratio in its RP precursor spectrum relative to that of **4G**. Nakajima et al.[96] were unable to detect an NI triplet EPR spectrum in their studies of NI-linked hairpins. This difference in behavior probably reflects the fact that the energy of ^{3*}NI (2.03 eV)[97] is above that of $G^{+\bullet}-NI^{-\bullet}$ (∼1.8 eV) while the energy of ^{3*}P (∼1.1 eV)[14] is well below that of $G^{+\bullet}-P^{-\bullet}$ (∼1.7 eV).

The magnitudes of $2J$ for **0G** and **4G** (Table 2) are all very small, implying that the noncovalent interactions of the RPs through the π-stacked base pairs are weak. At 85 K, the decrease in $2J$ for **0G** relative to that for **4G** may reflect a conformational change at the A-base trap site in **0G** that diminishes the π overlap of this A base with its adjacent bases; this may be

(87) Lewis, F. D.; Zhu, H. H.; Daublain, P.; Cohen, B.; Wasielewski, M. R. *Angew. Chem., Int. Ed.* **2006**, *45*, 7982–7985.
(88) Lewis, F. D.; Wu, T.; Zhang, Y.; Letsinger, R. L.; Greenfield, S. R.; Wasielewski, M. R. *Science* **1997**, *277*, 673–676.
(89) Giese, B.; Amaudrut, J.; Kohler, A. K.; Spormann, M.; Wessely, S. *Nature* **2001**, *412*, 318–320.
(90) Kendrick, T.; Giese, B. *Chem. Commun.* **2002**, 2016–2017.
(91) Grozema, F. C.; Tonzani, S.; Berlin, Y. A.; Schatz, G. C.; Siebbeles, L. D. A.; Ratner, M. A. *J. Am. Chem. Soc.* **2008**, *130*, 5157–5166.
(92) Conwell, E. M.; Rakhmanova, S. V. *Proc. Natl. Acad. Sci. U.S.A.* **2000**, *97*, 4556–4560.
(93) Conwell, E. M.; Park, J.-H.; Choi, H.-Y. *J. Phys. Chem. B* **2005**, *109*, 9760–9763.
(94) Barnett, R. N.; Cleveland, C. L.; Joy, A.; Landman, U.; Schuster, G. B. *Science* **2001**, *294*, 567–571.
(95) Renger, T.; Marcus, R. A. *J. Phys. Chem. A* **2003**, *107*, 8404–8419.
(96) Nakajima, S.; Akiyama, K.; Kawai, K.; Takada, T.; Ikoma, T.; Majima, T.; Tero-Kubota, S. *ChemPhysChem* **2007**, *8*, 507–509.
(97) Wiederrecht, G. P.; Svec, W. A.; Wasielewski, M. R.; Galili, T.; Levanon, H. *J. Am. Chem. Soc.* **1999**, *121*, 7726–7727.

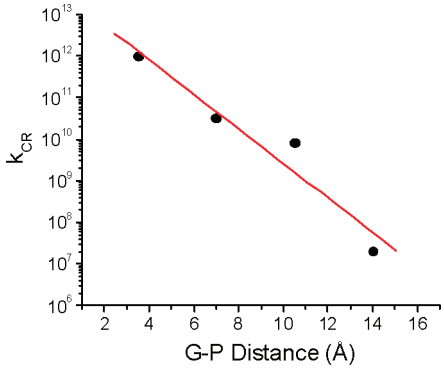

Figure 6. Distance dependence of the $(A_3)-P^{-\bullet}-(A_n)-G^{+\bullet}$ charge-recombination rate in **1G**−**4G**.

responsible for polaron trapping at that site. The value of $2J$ depends exponentially on the distance between the two radical ions, so $2J$ is small when the distance r is large and can be described by[98]

$$2J = 2J_0 e^{-\alpha(r-r_0)} \tag{6}$$

where $2J_0$ is the spin−spin exchange interaction at van der Waals contact, α is a constant, and r_0 is the van der Waals contact distance of ∼3.5 Å. The spin−spin exchange interaction $2J$ is directly proportional to the electronic-coupling matrix element V^2 for the charge-recombination reaction.[99−101] In turn, electron-transfer theory shows that the rate constant k_{CR} for charge recombination is also directly proportional to V^2,[102,103] so the values of $2J$ can be used to estimate V_{CR}, the electronic-coupling matrix element for charge recombination, and thereby predict the charge-recombination rates. Since the energy of $(A_3)-P^{-\bullet}-(A)_3-G^{+\bullet}$ is ∼0.4 eV below that of $(A_3)-P^{-\bullet}-(A_3)^{+\bullet}-G$ and $(A_3)^{+\bullet}-P^{-\bullet}-(A_3)-G$, thermal detrapping of $G^{+\bullet}$ is expected to be strongly activated; this means that charge recombination most likely occurs via a single-step superexchange mechanism, as previously proposed for stilbene−G RPs.[104] The rates of electron-transfer reactions proceeding by the superexchange mechanism also exhibit an exponential distance dependence identical in form to that of eq 6:

$$k_{ET} = k_{ET}^0 e^{-\beta(r-r_0)} \tag{7}$$

Thus, the exponential damping factor β for the distance dependence of the charge-recombination rate in eq 7 is equal to α in eq 6. A plot of log k_{CR} versus distance for **1G**−**4G** is presented in Figure 6. The slope of this plot provides a β value of 1.0 $Å^{-1}$, which is similar to the values reported for charge recombination in stilbene-linked hairpins.[104]

Consideration of the spin-selective charge-recombination pathways leading to the ground state and to $^{3*}P$ shows that $2J$ is related to V_{CR} by the approximate expression[100,101,105,106]

$$2J = \frac{V_{CR}^{\ 2}}{\Delta G_{CRT} + \lambda} - \frac{V_{CR}^{\ 2}}{\Delta G_{CRS} + \lambda} \tag{8}$$

in which ΔG_{CRT} and ΔG_{CRS} are the charge-recombination free energies for the triplet and singlet, respectively, and λ is the total reorganization energy for charge recombination, given by $\lambda = \lambda_I + \lambda_S$, where λ_I and λ_S are the reorganization energies of the RP and solvent, respectively. V_{CR} and λ are assumed to be equal for charge recombination to both the ground state and $^{3*}P$.[106] The values $\lambda_I = 1.0$ eV and $\lambda_S = 0.2$ eV were determined previously for charge recombination in a series of contact RPs within DNA hairpins.[86] Using the data for **4G** at 295 K ($\Delta G_{CRS} = -1.7$ eV, $\Delta G_{CRT} = -0.6$ eV, $2J = 0.08$ mT $= 4 \times 10^{-5}$ cm^{-1}, and $\lambda = 1.2$ eV) in eq 8 yields $V_{CR} = 0.3$ cm^{-1}. These parameters can be used to calculate k_{CR} via the following semiclassical expression from electron-transfer theory (valid for one quantum mode):[102,103,107]

$$k_{CR} = \frac{2\pi}{\hbar}|V_{CR}|^2 \sqrt{\frac{1}{4\pi\lambda_S k_B T}} \sum_{n=0}^{\infty} \exp(-S)\frac{S^n}{n!} \exp\times \left[-\frac{(\Delta G_{CR} + \lambda_S + n\hbar\omega)^2}{4\lambda_S k_B T}\right] \tag{9}$$

where $\hbar\omega$ is the vibrational quantum, assumed to be 1500 cm^{-1}, and $S = \lambda_I/\hbar\omega$. Using the parameters noted above in eq 9 gives $k_{SS}^{CR} = 3 \times 10^7$ s^{-1} and $k_{TT}^{CR} = 4 \times 10^7$ s^{-1}, which agree reasonably well with the measured values $k_{SS}^{CR} = 1.2 \times 10^7$ s^{-1} and $k_{TT}^{CR} = 1.7 \times 10^7$ s^{-1} for **4G** (Table 2). Thus, the measured values of $2J$ provide a direct estimate of the electronic-coupling matrix element for charge recombination of the RP through the π-stacked base pairs within the DNA hairpin. This approach should prove useful in analyzing the corresponding electronic couplings within other π-stacked supramolecular arrays.

Conclusions

P is a photooxidant that is sufficiently powerful to quantitatively inject holes into adjacent A and G nucleobases. The charge-transfer dynamics observed following hole injection from P into the A-tract of the DNA hairpins is consistent with formation of a polaron involving an estimated 3−4 A bases. Trapping of the $(A_{3-4})^{+\bullet}$ polaron by a G base at the opposite end of the A-tract from P is only competitive with charge recombination of the polaron and $P^{-\bullet}$ at short P−G distances. In a hairpin having 3 A−T base pairs between P and G (**4G**), the radical ion pair that results from trapping of the hole by G is spin-correlated and displays a TREPR spectrum at 295 K that is consistent with its formation from $^{1*}P$ by the RP-ISC mechanism. A similar spectrum for **4G** with very similar values of $2J$ and D is observed at 85 K. In addition, charge recombination is spin-selective and produces $^{3*}P$, which at 85 K exhibits a spin-polarized TREPR spectrum that is diagnostic for its origin from a precursor radical ion pair formed by the RP-ISC mechanism. No comparable spectra are observed when only one A−T base pair is between P and G (**2G**) because of rapid charge recombination. Interestingly, TREPR spectra of a hairpin having

(98) De Kanter, F. J. J.; Kaptein, R.; Van Santen, R. A. *Chem. Phys. Lett.* **1977**, *45*, 575–579.
(99) Anderson, P. W. *Phys. Rev.* **1959**, *115*, 2–13.
(100) Feher, G.; Okamura, M. In *Tunneling Conference*; Chance, B., Devault, D., Frauenfelder, H., Marcus, R. A., Schreiffer, J. R., Sutin, N., Eds.; Academic Press: New York, 1979; pp 729−743.
(101) Nelsen, S. F.; Ismagilov, R. F.; Teki, Y. *J. Am. Chem. Soc.* **1998**, *120*, 2200–2201.
(102) Marcus, R. A. *J. Chem. Phys.* **1965**, *43*, 679–701.
(103) Jortner, J. *J. Chem. Phys.* **1976**, *64*, 4860–4867.
(104) Lewis, F. D.; Wu, T. F.; Liu, X. Y.; Letsinger, R. L.; Greenfield, S. R.; Miller, S. E.; Wasielewski, M. R. *J. Am. Chem. Soc.* **2000**, *122*, 2889–2902.
(105) Kobori, Y.; Sekiguchi, S.; Akiyama, K.; Tero-Kubota, S. *J. Phys. Chem. A* **1999**, *103*, 5416–5424.
(106) Weiss, E. A.; Ratner, M. A.; Wasielewski, M. R. *J. Phys. Chem. A* **2003**, *107*, 3639–3647.

no G bases (**0G**) at 85 K revealed a spin-correlated radical pair with a *D* value identical to that of **4G**. This implies that an A base in a unique environment in the fourth A−T base pair from the P chromophore serves as a hole trap at 85 K. Our data suggest that hole injection and transport in these hairpins is completely dominated by polaron generation and movement to a trap site rather than by superexchange. On the other hand, charge injection from $G^{+\bullet}$ back onto the A−T base pairs is strongly activated, so charge recombination from G (or even A trap sites at 85 K) most likely proceeds by a superexchange mechanism.

Acknowledgment. This work was supported by the National Science Foundation under Grant CHE-0628130.

Supporting Information Available: Additional data on DNA hairpin characterization, fluorescence quantum yields, transient absorption data, and complete ref 59. This material is available free of charge via the Internet at http://pubs.acs.org.

JA803765R

(107) Hopfield, J. J. *Proc. Natl. Acad. Sci. U.S.A.* **1974**, *71*, 3640–3644.